Mehran University Research Journal of Engineering and Technology

https://doi.org/10.22581/muet1982.3145

2024, 43(4) 116-129

Green synthesis of ZnO/Fe_3O_4 nanoparticles with nigella sativa extract: Efficient degradation of methylene blue and antimicrobial properties

Noor Ali Bhanoojo [a], Mohammad Younis Talpur [a, *], Sarfaraz Ahmed Mahesar [b], Syeda Sara Hassan [c], Ume Hanee Nadeem Ahmed [a], Fatih Durmaz [d]

[a] *Dr. M. A. Kazi Institute of Chemistry, University of Sindh, Jamshoro, 76080, Sindh, Pakistan*

[b] *National Center of Excellence in Analytical Chemistry, University of Sindh, Jamshoro, 76080, Sindh, Pakistan*

[c] *US-Pakistan Center for Advanced Studies in Water (USPCASW), Mehran University of Engineering and Technology, Jamshoro, 76062, Sindh, Pakistan*

[d] *Department of Chemistry, Selcuk University, Konya 42075, Turkey*

[*] Corresponding author: Mohammad Younis Talpur, Email: younis.talpur@usindh.edu.pk

Received: 08 January 2024, Accepted: 27 September 2024, Published: 01 October 2024

KEYWORDS

Biogenic Synthesis

ZnO NPs

Fe_3O_4 NPs

ZnO/Fe_3O_4 NCs

Catalytic Degradation

Antimicrobial Activity

ABSTRACT

Zinc oxide (ZnO), iron oxide (Fe_3O_4) NPs, and ZnO/Fe_3O_4 nanocomposites (NCs) were synthesized using Nigella sativa (NS) seed extracts. These nanomaterials (NMs) were characterized by multiple analytical techniques like UV-visible spectrophotometers, FTIR spectroscopy, SEM, and XRD spectroscopy. The UV-visible spectrum showed 364 nm, 330 nm, and 331nm for ZnO NPs, Fe_3O_4 NPs, and ZnO/Fe_3O_4 NCs, respectively. Moreover, it was confirmed when the samples were run through FTIR techniques, and it was observed that the availability of bioactive functional groups was involved in the decline of bulk compounds to NPs. XRD showed their average nanoparticle size based on applying the formula of full width at half maximum (FWHM) for ZnO NPs, Fe_3O_4 NPs, and ZnO/Fe3O4NCs at 29.52 nm, 22.08 nm, and 12.82 nm, respectively. In this study, NPs and NCs reduced Methylene Blue (MB) dye, and a UV-visible spectrophotometer investigated their catalytic activities. MB dye showed the maximum absorption peak at 664 nm. The reaction of MB was reduced using synthesized products with an accompanying color change reaction from blue to colorless within 60 min at 84%, 86%, and 99.5% degradation for ZnO NPs, Fe_3O_4 NPs, and ZnO/Fe_3O_4 NCs with rate constants of 0.00035, 0.00065, and 0.0015 Lmol-1S-1. The 2nd order rate constant was observed in this study. The agar disc diffusion method was used to investigate the potential antibacterial activity of synthesized NPs and NCs. This study is best suited for Gram-positive bacteria. NS seed extract-based synthesis of NCs could be an excellent catalyst and biological application for environmental pollution.

1. Introduction

Nanotechnology deals with nanoparticles related to atomic or molecular aggregates and characterized by a size of less than 100 nm. Nanoparticles are made from different substances. Nanoparticles are essential because of their fascinating properties and multiple applications [1]. Nanoparticles also have the unique property that their surface area increases as per unit volume. This increased surface area allows these nanoparticles to behave differently from their bulk-size counterparts. Bulk metal is initially inactive, but when converted into NPs, it shows some other unique properties, such as high reactivity [2]. Biogenic synthesis of metal oxide nanoparticles is unique for

antibacterial, antimicrobial, biomedical, and so on catalysts. This study used the biogenic synthesis route for metal oxide nanoparticles. Nigella sativa (NS) is a naturally flowering plant in the Ranunculaceae family. NS seeds are also known by another name, black cumin seeds, as shown in Fig 1.

Fig. 1. Image Of Nigella Sativa Flower And Its Seed

NS flowering plants have many energetic compounds, such as proteins, flavonoids, terpenoids, alkaloids, tannins, ketones, aldehydes, and carboxylic acids. These energetic compounds may act as reducing agents in the synthesis of NPs [3].

NS is essential in activities related to biological factors and therapeutic potential. It possesses a broad spectrum of activities such as antidiabetic, anti-cancer, antihypertensive immunomodulatory, diuretic, analgesic, antimicrobial, antihelminthic, analgesics and anti-inflammatory, mitigate liver injury, spasmolytic, bronchodilator, gastroprotective, kidney protective, and antidote properties [4]. NS is regarded as the primary source of nutritionally necessary components. Its oil includes various phytochemicals, including polyunsaturated fatty acids (PUFA), with potent antioxidant effects and lower sucrose levels [5, 6]. NS plant extract method has shown more and more cogitation in nanotechnology due to its minimum cost, maximum efficiency, no morbidity, and eco-friendliness. [7]. NS extracts are used in conventional medicine to treat many diseases, like dermis infection, stomach and heart conditions, pneumonic illnesses, infections, *etc.* [8]. However, the seeds and oils of NS are well known for their most effective activities, like anti-cancer, antimicrobial resistance, anti-inflammatory, antioxidant, and stomach protective activities [9].

The root cause of water contamination is gradually increasing environmental pollution. When organic dyes are released from various textile industries, which make water pollutants, they are caught by different diseases due to the polluted water utilized by humans and other animals. And the aquatic ecosystem is also being affected by polluted water. The ZnO nanostructures have many applications in multiple fields, like ultra-violet lasers, energy transmutation, gas sensors, enzymes, and information related to the biomedical sciences [10]. Furthermore, several active methods, such as deactivation techniques, have been established to lessen water pollutants. These methods include filtration, adsorption, alleviation, and biological treatment, but these all methods have many side effects on our ecosystem and are not acceptable for the extensive terminal of pollutants to make water purified; hence, there is too much need to make pure and cost-effective water purification techniques [11, 12].

Industries producing textile materials like paper, plastics, leather, food, and cosmetics also have negative feedback, making the environment polluted for living organisms [13, 14]. Industrial effluents contain harmful substances, such as dyes, heavy metals, phenolic compounds, and pharmaceuticals; harmful substances negatively affect the ecosystem [15]. As we know, water free from harmful substances is a basic need for humans and other living organisms to improve their health and survival. Still, globally, it is observed that most countries have difficulties due to the inadequacy of clean drinking water [16, 17].

Many metal oxide nanoparticles, like ZnO, Fe_3O_4, TiO2, CuO, *etc.*, are being used to degrade harmful organic/inorganic dyes from different water sources [18]. ZnO NPs' strong oxidation capabilities, large surface area to volume ratio, small particle size, and adequate band gap energy of 3.37 eV all contribute to their important role in eliminating organic dyes from industrial wastewater [19, 20].

Magnetite Fe_3O_4 is a most important member of magnetic nanomaterials; recently, many practical applications have been introduced, such as catalysis, magnetic storage media, magnetic field-assisted separations and analyses, targeted drug delivery, and different agents in magnetic resonance imaging (MRI) [21]. At present, non-toxic, environmentally friendly solvents/chemicals are used, and renewable materials (ionic liquid) are the most beneficial because having a great interest in a friendly ecosystem leads to green chemistry [22, 23].

We also know that the metal oxides surface defects and interface properties are significant in their catalytic activities [24, 25]. Due to their optical qualities, distinct magnetic characteristics, photochemical capabilities, electrical properties, and catalytic properties, magnetic nanoparticles (NPs) have demonstrated the most significant and intriguing scientific challenges at this time [26]. The excellent

magnetic characteristics of zinc-ferrite composite (ZnFe3O4) give it limitless demand. Zinc ferrite composites, or ZnFe3O4, are used in many applications, including gas sensors, semiconductor photo-catalysts, anode materials for lithium-ion batteries, and catalysis [27]. In response to various gases, such as acetone and ethanol vapors, the ZnFe2O4 NPs have demonstrated selectivity, adaptability, and high sensitivity. The following are some additional uses for ZnFe2O4NCs: because of their superior electrochemical qualities, which include good cycling performance, high reversible specific capacity, high specific capacity, and good rate accomplishment, these NCs are employed as electrode material for lithium-ion batteries (LIBs) [28].

In this study, we synthesized stable, small-sized ZnO/Fe_3O_4NCs using NS seeds extract. NS itself served as a capping and reducing agent to promote the formation of environmentally acceptable NCs. To my knowledge, ZnO/Fe_3O_4NCs of NS extract have not been studied against azo dye degradation and antibacterial resistance from wastewater effluents.

2. Experimental

2.1 Chemicals And Reagents

All the chemicals and reagents were used of Analytical Grade. Zinc acetate (99.999%), Iron (III) chloride hexahydrate ($FeCl_3.6H_2O$, 97.0%), Iron (II) chloride ($FeCl_2$, $4H_2O$, 99.99%), and Sodium hydroxide (NaOH, 97.0%) were purchased from Sigma Aldrich, USA. NS seed extract was purchased from the local market in Hyderabad, Sindh, Pakistan, and was used as a reducing/capping agent for synthesizing NPs and NCs. Deionized water collected from NCEAC, University of Sindh, Jamshoro, was used as a solvent throughout the research.

2.2 Analytical Techniques

In this study, we used different analytical techniques such as UV-visible spectrophotometers, Fourier transforms infrared (FTIR) spectroscopy, scanning electron microscopy (SEM), and X-ray diffraction (XRD) spectroscopy for the characterization of green synthesized ZnO, Fe_3O_4, and their nanocomposites (Fe_3O_4/ZnO).

2.2.1 UV-Visible study

UV-visible shows the bonding patterns from electronic transitions in size, structure, and composition. We tested the synthesized sample on a UV-visible spectrophotometer for the initial checkup. The UV-visible spectrophotometer covered the 800-200 nm range.

2.2.2 Fourier transforms infrared (FTIR) study

The synthesized NPs and NCs were run through FTIR spectroscopy to determine the functional groups. The synthesized NMs were scratched, collected, and processed in KBr pellets for FT-IR studies.

2.2.3 Scanning electron microscopy (SEM) study

Prepared samples were run through the SEM micrographs to understand the surface morphology of green synthesized ZnO, Fe_3O_4, and Fe_3O_4/ZnO NMs.

2.2.4 X-ray diffraction (XRD) study

The XRD technique determined the phase composition and crystalline structure of green synthesized NMs.

2.3 Methods

2.3.1 Preparation of extract

NS seed extract was prepared by crushing the seed in a grinder. NS seed powder was washed thoroughly with distilled water. After that, 10g of the prepared powder form of the sample was homogenized in 50 ml of distilled water, and then incubation was performed at 80 °C for 20 min while the incubation sample was under constant stirring at 100 rpm. After that, the obtained product was filtered through 0.2 μm filter paper to remove more impurities. After filtration, the sample was kept at 4 °C for further experiments. Finally, NS seed extract was used to synthesize ZnO NPs, Fe_3O_4 NPs, and Fe_3O_4/ZnO NCs.

2.3.2 Green synthesis of ZnO NPs

ZnO NPs were prepared by using NS seed extract. A zinc acetate (0.1M) solution was prepared, and then a 7:3 ratio of zinc acetate and extract was mixed. After that, the pH of the mixture was maintained at 10, and the mixture was kept on a hot plate for 20 minutes at 80^{o}C with a constant speed of 300 rpm. After that, the color of the mixture was changed from brownish-yellow to white, representing and confirming the formation of ZnO NPs. In the next step, the solution was kept to get cooled. After that, the solution was filtered and made transparent for the UV-visible technique. The synthesized NPs were washed with deionized water to remove impurities and then dried in a petri dish by some heating. The solid ZnO NPs were collected by scratching a petri dish and stored at 4 C for further characterization.

2.3.3 Green synthesis of Fe_3O_4 NPs

The stock solutions were initially prepared as Fe (II) and Fe (III) were prepared by taking their molarities at

0.1 M and 0.2 M molar concentrations, respectively. After that, both solutions were added in 1:1 ratios (3.5 ml of Fe(III) and 3.5 ml of Fe(II), and then the mixture of both solutions (7 mL) was mixed with 3 ml of NS extract in ratios 7:3. Then 1M NaOH was added dropwise to the sample, and gradually the pH of the mixture was checked, and the pH of the solution was brought to 10. Then, the mixture was kept at 80 °C, vigorously stirring for 20 minutes. The mixture was then cooled and allowed to form until the black precipitate formed. In the next step, the resultant nanoparticle solution was purified by centrifugation at 10,000 rpm for 12 minutes to make the solution transparent for the UV-visible technique. The synthesized NPs were washed with deionized water to remove impurities and then dried in a petri dish by some heating. The solid Fe_3O_4 NPs were collected by scratching from Petri dishes and stored at 4°C for further characterization.

2.3.4 Green synthesis of ZnO/Fe_3O_4 NCs

To synthesize ZnO/Fe_3O_4NCs, 5 mL were taken from the prepared sample of ZnO NPs and 5 mL from the prepared sample of Fe_3O_4 NPs as ratios (1:1). Both solutions were mixed homogeneously. After that, from the mixture of both solutions, 8 mL was mixed with 2 mL of NS extract and added to the NaOH solution to bring the pH to the primary medium. NaOH was added until the pH of the solution approached the basic medium pH 10. The mixture was then vigorously stirred at 80 °C for 20 minutes, and then the mixture was cooled and allowed to form until the yellow-brown precipitate formed. In the next step, the resultant NC's solution was purified by centrifugation at 10,000 rpm for 12 mins to make the solution transparent for the UV-visible technique. The synthesized NCs were washed with deionized water to remove impurities and then dried in a petri dish by some heating. The solid ZnO/Fe_3O_4NCs were collected by scratching from Petri dishes and stored at 4°C for further characterization.

2.3.5 Catalytic degradation of methylene blue (MB)

MB is a common organic pollutant in wastewater from the dyeing and printing industries. Organic dyes: MB is an azo dye with benzene rings that is toxic and durable in the environment. MB is a cationic dye that is soluble in water. The catalytic activity of the synthesized NMs (ZnO NPs, Fe_3O_4 NPs, and ZnO/Fe_3O_4 NCs) was comparatively estimated in the presence and absence of sodium borohydride (1 mL, 0.5 M $NaBH_4$). Firstly, an MB solution (25 mL, 100 mg/L) was treated with the synthesized NMs (0.2 mg) without $NaBH_4$. The results were obtained with negligible effect. The progress of the catalytic reduction was assessed using the UV-visible technique, and an absorption peak was found at λmax = 664 nm. Then, the MB solution was treated with the synthesized NMs in the presence of $NaBH_4$. The results were proved by quickly vanishing the MB distinct absorption peak at 664 nm.

2.3.6 Antimicrobial activity

The agar-well diffusion method was used to measure the antibacterial activity. Nutrient agar medium was made for bacteria, and potato dextrose agar medium was used for Candida. Subsequently, the two were transferred onto 25 mL Petri dishes and hardened for 60 minutes. Next, wells were cut in the growing media using a sterile cork borer (6 mm). Afterward, suspensions of the strains above bacterial or Candida medium (tuned to 0.01 optical density) were added to a sterilized piece of cotton (a swab). At a 50mg/mL concentration, a cotton swab was streaked over the growing medium to immunize agar plates. Sterile distilled water was used to prepare 50 μl of the tested samples. Subsequently, the plates were incubated for 48 hours at 37 °C using light energy provided by LEDs. A meter scale was used to quantify the growth inhibition zone sizes. In this study different ratios of samples were taken; Gram +ve at 1 ratio of ZnO NPs/distilled water 2:2; at 2 ratios of ZnO NPs/distilled water 3:1; at 3 ratios of Fe_3O_4 NPs/distilled water 2:2; at 4 ratios of Fe_3O_4 NPs/distilled water 3:1; at 5 ratios of ZnO/Fe_3O_4 NCs/distilled water 2:2; at 5 ratios of ZnO/Fe_3O_4 NCs/distilled water 3:1; from these all the cultural media of the Mueller Hinton Agar (M.HA) where all synthesized samples were applied. Prepared samples were applied on cultural media of Mueller Hinton Agar (M.HA) of gram-ve *Escherichia coli* (*E. coli*) and gram+ve *Staphylococcus aureus* (*S. aureus*), respectively.

3. Results and Discussion

3.1 UV-Visible Study of ZnO, Fe_3O_4 NPs and ZnO/ Fe_3O_4NCs

3.1.1 UV-Visible study of ZnO NPs

Fig. 2a displays the synthesized greener ZnO NPs' UV-visible absorption spectra. The Prepared sample was run through the UV-visible technique, and the peak was 364 nm [29]. It represents that ZnO NPs were prepared.

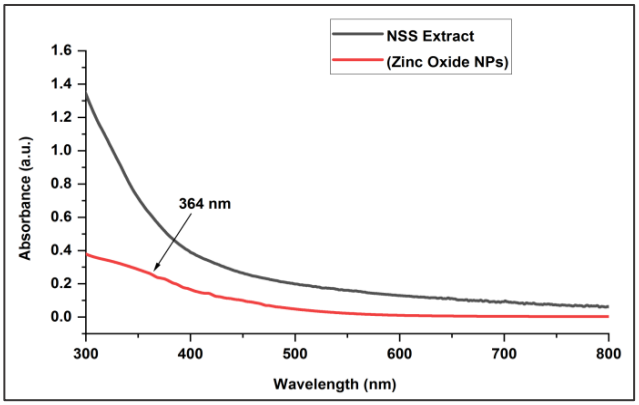

Fig. 2a. UV–Visible Absorption Spectrum Of Synthesized ZnO NPs

3.1.2 UV-Visible study of Fe_3O_4 NPs

Fig. 2b displays the synthesized nanoparticle spectra of UV-visible absorption. The Prepared sample was run through the UV-visible technique, and the peak was observed as 330 nm [30]. It represents that Fe_3O_4 NPs were prepared.

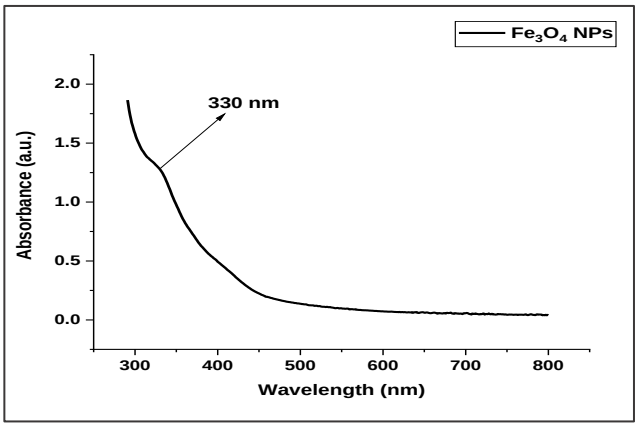

Fig. 2b. UV–Visible Absorption Spectrum Of Synthesized Fe_3O_4 NPs

3.1.3 UV-Visible study of ZnO/Fe_3O_4 NCs

The UV-visible absorption spectrum of synthesized nanoparticles is shown in Fig. 2c. The Prepared sample was run through the UV-visible technique, and the peak was observed at 331 nm [31]. It indicates that ZnO/Fe_3O_4 NCs were prepared.

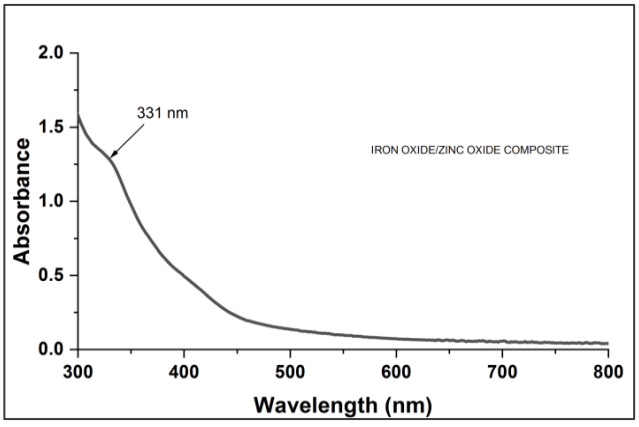

Fig. 2c. UV–Visible Absorption Spectrum Of Synthesized ZnO/ Fe_3O_4 NCs

3.2 Band Gap Study Of ZnO, Fe_3O_4 NPs and ZnO/ Fe_3O_4 NCs

3.2.1 Bandgap energy of ZnO NPs

ZnO NPs band gap energy was estimated by Eq. 1 to be roughly 3.39Ev, as shown in Fig. 3a. This value is consistent with research that has already been published. The following Eq. was utilized to predict the energy band gap of synthesized ZnO NPs:

$$E_g = hc/\lambda \quad (1)$$

E_g is band gap energy (eV), h is Plancks constant, c is light velocity, and λ is the wavelength at maximum absorbance (nm). From the above Eq., the band gap energy is calculated to be 3.39 eV. Additionally, the band gap widens when particle size decreases, as demonstrated by applying absorption spectroscopy. Band gap energy and absorption wavelength are also inverse [32].

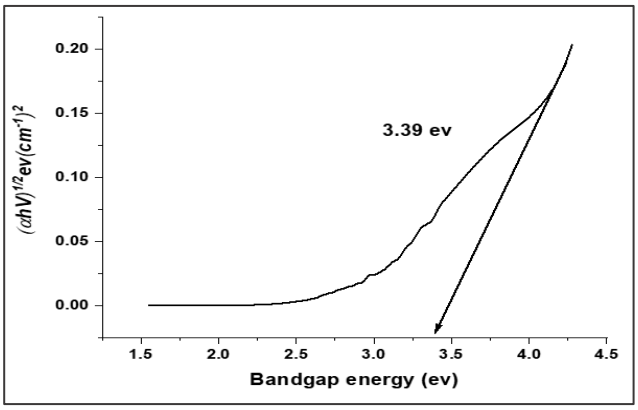

Fig. 3a. Band Gap Energy of ZnO NPs

3.2.2 Bandgap energy of Fe_3O_4 NPs

After several calculations, the band gap energy of Fe_3O_4 nanoparticles was approximately 2.88 eV. This band gap value denotes the presence of synthesized Fe_3O_4 nanoparticles. Eq. 1 was used to compute the band gap energy at the specified Fig. 3b. The literature has reported on the impact of surface shape and its connection to ZnO synergistic action [33].

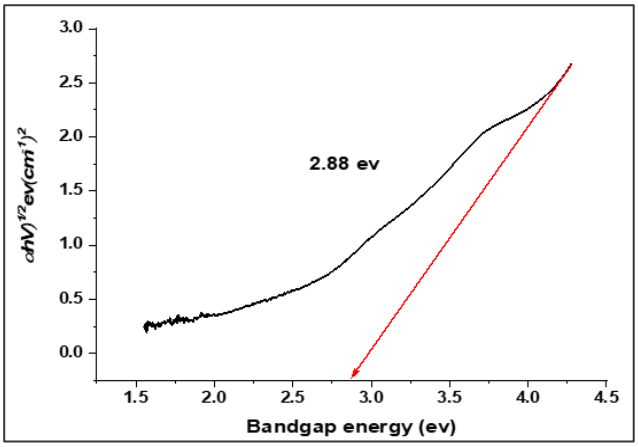

Fig. 3b. Band Gap Energy Of Fe_3O_4 NPs

3.2.3 Bandgap energy of ZnO/ Fe_3O_4 NCs

The band gap energy of ZnO/Fe_3O_4 NCs was calculated at about 2.91 eV by calculating multiple parameters using eq. 1 [34]. The given value of the band gap represents the presence of synthesized ZnO/ Fe_3O_4 NCs, as shown in Fig. 3c.

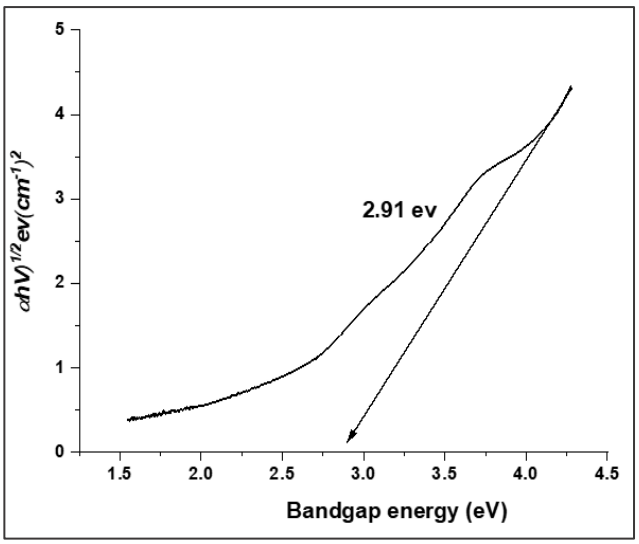

Fig. 3c. Band Gap Energy Of ZnO/Fe_3O_4 NCs

3.3 FTIR Study Of Green Synthesized ZnO, Fe_3O_4 NPs, and ZnO/Fe_3O_4 NCs

3.3.1 FTIR study of ZnO NPs

ZnO NPs FTIR spectra were recorded using the KBr pellet technique. ZnO and IR grade KBr were manually mixed in a 1:3 ratio to create the samples. The ZnO NPs FTIR spectra are shown in Fig. 4a. The Zn-O stretching vibrational mode of ZnO nanoparticles is attributed to the peak at 475.81 cm^{-1}. Some other additional peaks may be due to O-H, C-H, Alkenes, C-O, and amide.

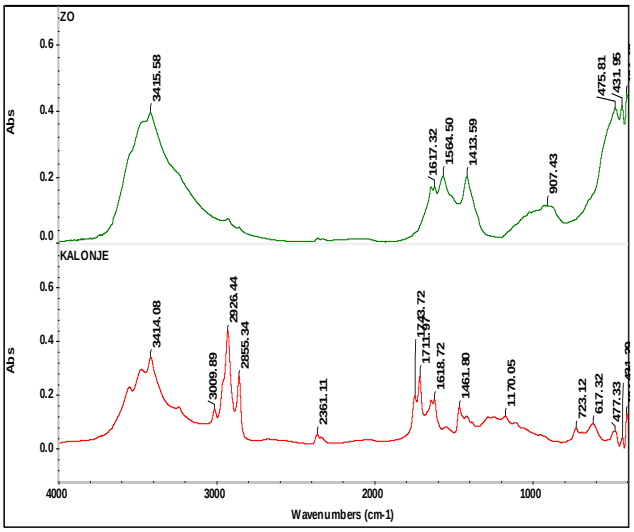

Fig. 4a. FTIR Spectrum of ZnO NPs

3.3.2 FTIR study of Fe_3O_4 NPs

Fe_3O_4 nanoparticle's FTIR spectra were recorded using the KBr pellet technique. The samples were made by manually combining Fe_3O_4 and IR grade KBr in a 1:3 ratio. The Fe_3O_4 NPs FTIR spectra are described in Fig. 4b. The Fe-O stretching vibrational mode of Fe_3O_4 NPs is attributed to the peak at 616.70 cm^{-1}. Some other additional peaks may be due to O-H, C-H, Alkenes, C-O, and amide.

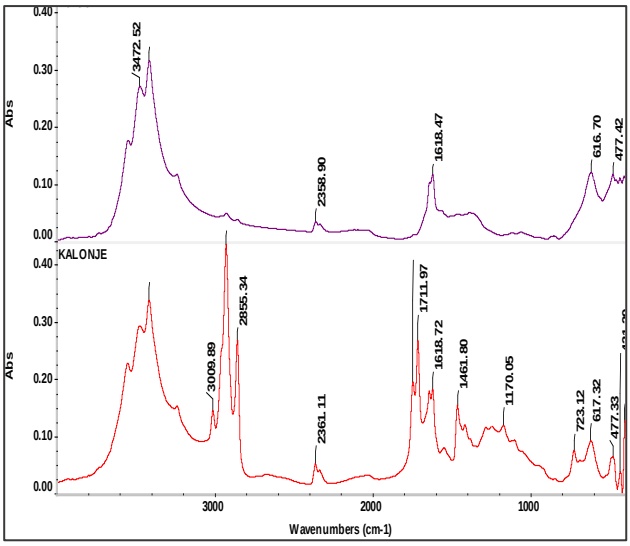

Fig.4b. FTIR Spectrum of Fe3O4 NPs

3.3.3 FTIR study of ZnO/Fe_3O_4 NCs

ZnO/Fe_3O_4 NCs FTIR spectra were recorded through the KBr pellet technique. The samples were made by manually combining ZnO/Fe_3O_4 NC with IR grade KBr in a 1:3 ratio. The FTIR spectra of ZnO/Fe_3O_4 NCs were explained in Fig. 4c. In ZnO/Fe_3O_4 NCs, the Zn-O and Fe-O stretching vibrational modes are attributed to the peaks at 477 and 616.70 cm^{-1}. Some other additional peaks may be due to O-H, C-H, Alkenes, C-O, and amide.

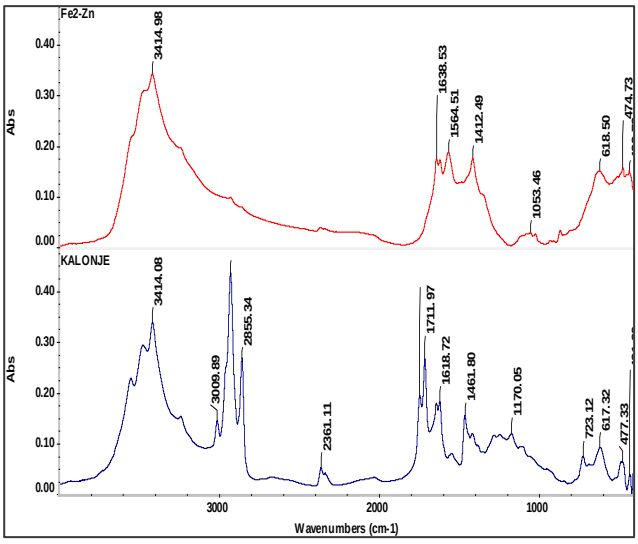

Fig. 4c. FTIR Spectrum of ZnO/Fe_3O_4 NCs

3.4. SEM Study Of Green Synthesized Nms

3.4.1 SEM study of ZnO NPs

The powder of ZnO NPs was prepared to study the surface morphology of ZnO NPs using SEM analysis.

The SEM image of ZnO NPs, as shown in Fig. 5a, reports a uniform distribution of nano-structural features that were formed and more agglomerated. ZnO NPs were also shown to be primarily horizontal in shape using the SEM technique, a finding that XRD further supported. Numerous scholarly works document the impact of surface shape and its correlation with ZnO synergistic action [35].

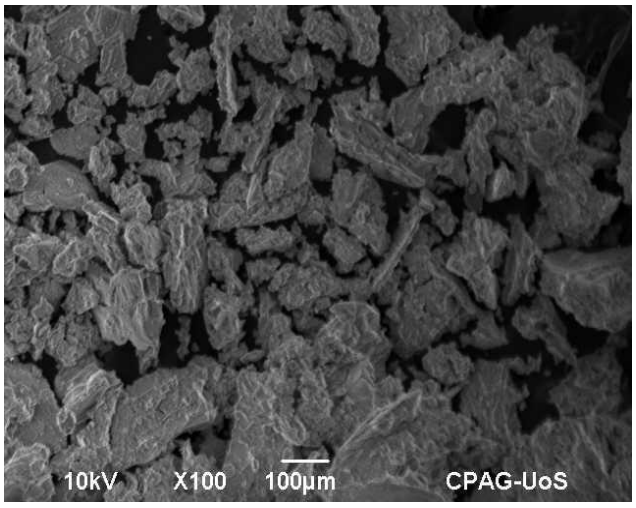

Fig. 5a. Surface Morphology of ZnO NPs by SEM

3.4.2 SEM study ofFe_3O_4 NPs

The prepared powdered Fe_3O_4 NPs surface morphology was studied using SEM analysis. The SEM image of Fe_3O_4 NPs is shown in **Fig.5b**, representing that the Fe_3O_4 NPs have an equal distribution of nano-structural features and are more agglomerated. The particles were mostly hexagonal-spinel in shape, and more confirmed samples were run through XRD [36].

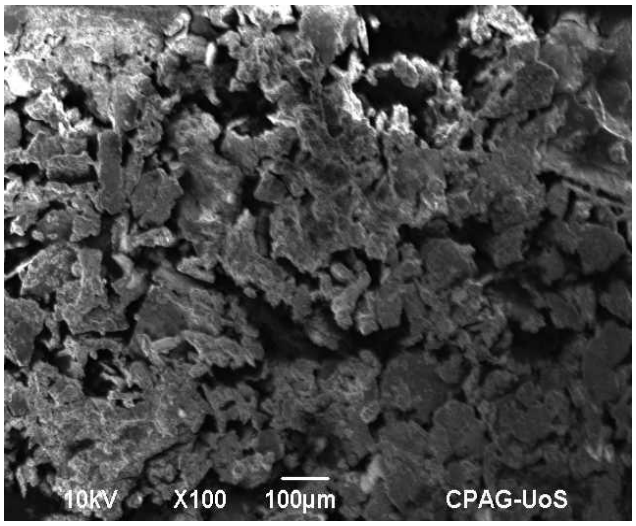

Fig. 5b. Surface Morphology of Fe_3O_4 NPs by SEM

3.4.3 SEM study of ZnO/ Fe_3O_4 NCs

The prepared powder of ZnO/ Fe_3O_4 NCs was run through the SEM for its morphology study. The morphology study observed that the synthesized ZnO/Fe_3O_4 NCs had mostly flat-like/agglomerated shapes, and a typical SEM image is depicted in Fig. 5c [37].

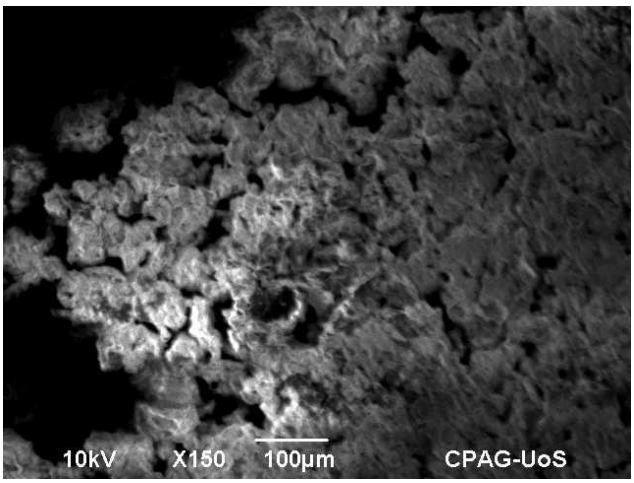

Fig. 5c. Surface Morphology of ZnO/Fe_3O_4 NCs by SEM

3.5. XRD Study Of Green Synthesized NMs

3.5.1 XRD study of ZnO NPs

The crystalline material of the ZnO NPs was used to analyze them using XRD, as shown in Fig 6a. The synthesized ZnO NPs were analyzed under XRD; they synthesized ZnO NPs showed peaks at values of 18°, 24°, 30°, 36.3°, 42.5°,47°, 57.7°, and 62.9° which were typical for the ZnO structure. The synthesized NPs were found to be hexagonal close-packed (HCP) in nature. The marked line of the diffraction peaks indicates that the synthesized materials are in the nanometer range. By using the Debye- Scherrer formula ($D = 0.9\ \lambda\ /\ \beta\ \cos\theta$), particle size was calculated, where θ is the diffraction angle, λ = 1.5406 Å, and β is the peak at half maximum. The average crystallite size of prepared ZnO NPs was calculated using the following eq.2, as mentioned in Fig. 6b [38].

$$D = \frac{0.89\lambda}{\beta\ (\mathrm{Cos}\theta)} \qquad (2)$$

From the Histogram, the average particle size was found at 29.52 nm.

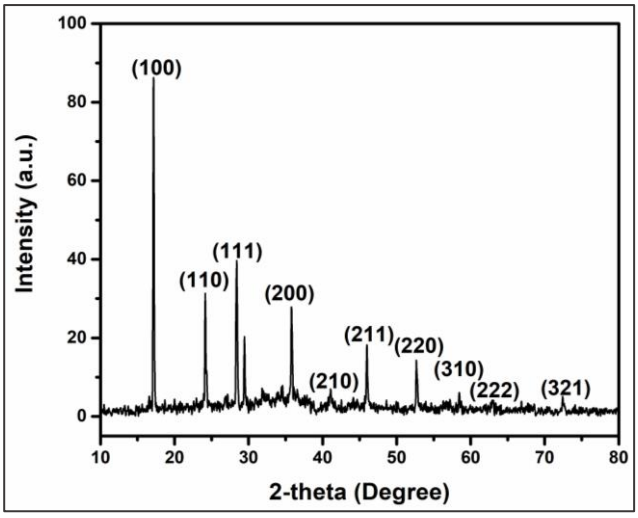

Fig. 6a. XRD Patterns of ZnO NPs

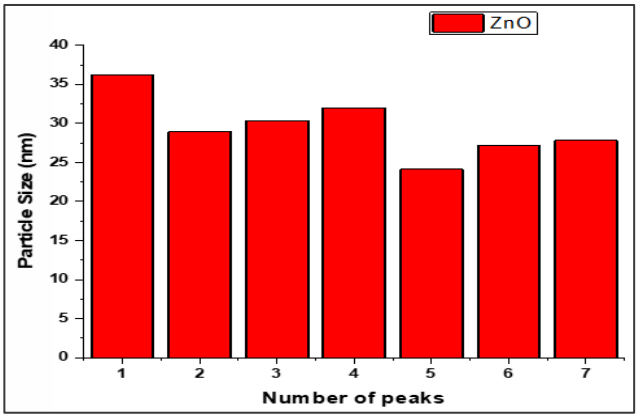

Fig. 6b. Histogram of ZnO NPs By XRD

3.5.2 XRD study ofFe_3O_4 NPs

The XRD pattern of the synthesized Fe_3O_4NPs showed peaks at different values of 28.5º, 33º, 37.6º, 46.3º, 58.5º, 69º, and 78º which are typical for the Fe_3O_4 structure as shown in Fig 7a. These firm peaks indicated the hexagonal shape of synthesized NCs. The synthesized materials are in the nanoscale range, as indicated by the line of the diffraction peaks. Using Scherrer's Eq. in the previously cited Eq. 2, the average particle was calculated using the diffraction peaks full width at half maximum (FWHM) [39]. The Histogram shows that the average particle size was 29.52 nm, as shown in Fig. 7b.

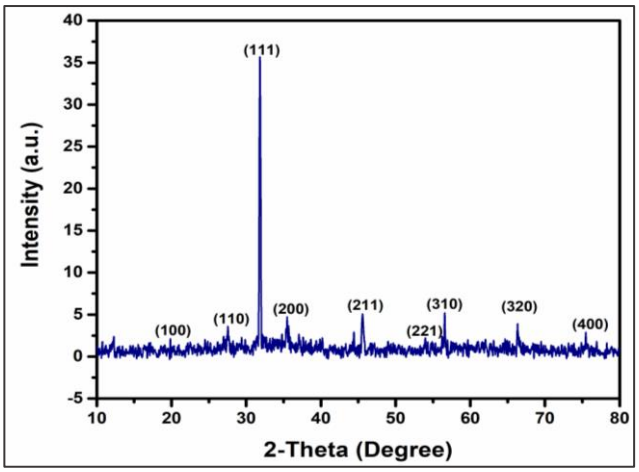

Fig. 7a. XRD Patterns of Fe_3O_4 NPs

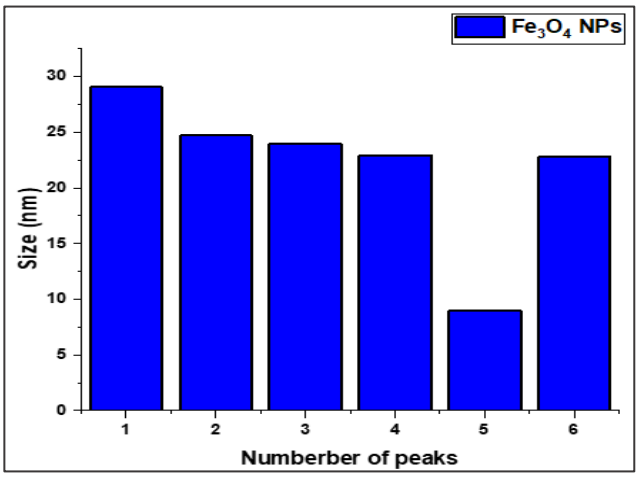

Fig. 7b. Histogram of Fe_3O_4 NPs By XRD

3.5.3 XRD study of ZnO/Fe_3O_4 NCs

The ZnO/Fe_3O_4 structure, as shown in Fig. 8a, is typical of the peaks that the synthesized ZnO/Fe_3O_4 NCs XRD reveals at values of 31º, 46º, 58.7º, 78º, and 75º. The marked line of the diffraction peaks indicates the range of nanometers for the synthesized materials. Scherrer's Eq. computed the diffraction peak's average particle size using the FWHM. This value is t = 0.9 ϒ/ (B cosθ). The X-ray's wavelength, ϒ, and its full width at half maximum, B, are given. These firm peaks indicated the hexagonal crystalline nature of synthesized NCs [40]. From the Histogram, the average particle size was 12.82 nm, as represented in Fig. 8b.

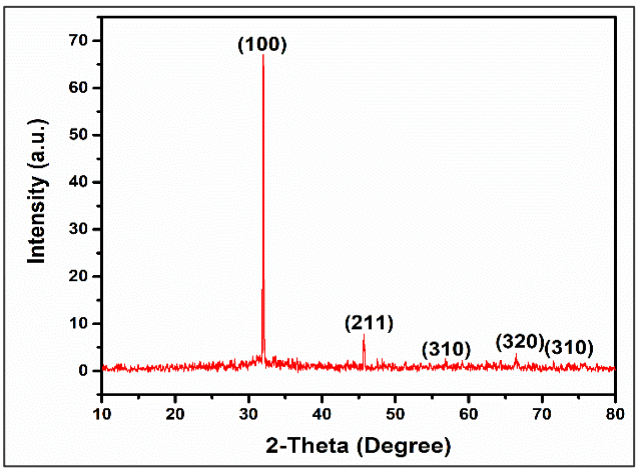

Fig. 8a. XRD Patterns of ZnO/Fe_3O_4 NPs

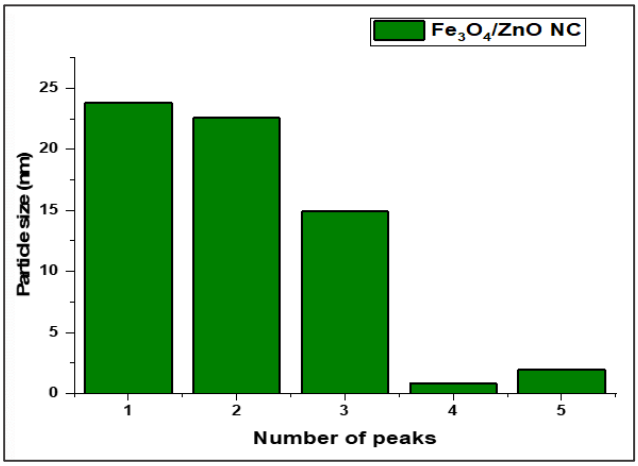

Fig. 8b. Histogram of ZnO/Fe_3O_4 NPs By XRD

3.6 Catalytic Degradation Of Methylene Blue (MB) Dye Using Green Synthesized NMs

3.6.1 p*H Factor*

pH is the most significant factor that tests the ability of a material. In this study, the effect of pH was observed, as shown in Fig. 9 (a-c). In this study, acidic medium pH=2, neutral medium pH=7, and basic medium pH=10 were the results of these individual results. The result at basic medium pH=10 showed the highest degradation at 99.5% [41]. The catalytic activity of the synthesized NMs was comparatively

estimated in the presence and absence of sodium borohydride (1 mL, 0.5 M $NaBH_4$). Firstly, an MB solution (25 mL, 100 mg/L) was treated with the synthesized NMs (0.2 mg) in the presence of $NaBH_4$ obtained at pH 2, 7, and 10, respectively.

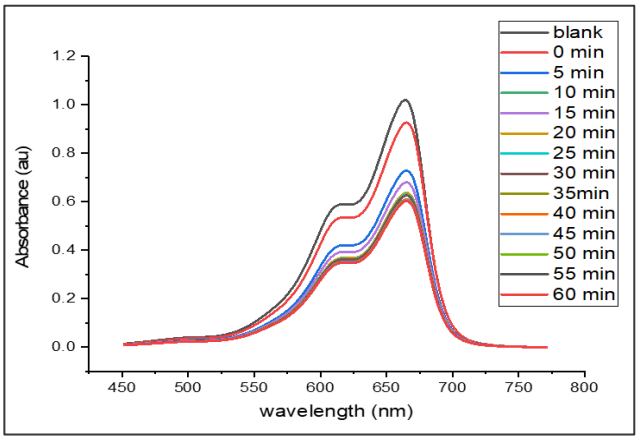

Fig. 9a. Degradation Of Methylene Blue Dye At pH=2 using ZnO/Fe_3O_4 NCs

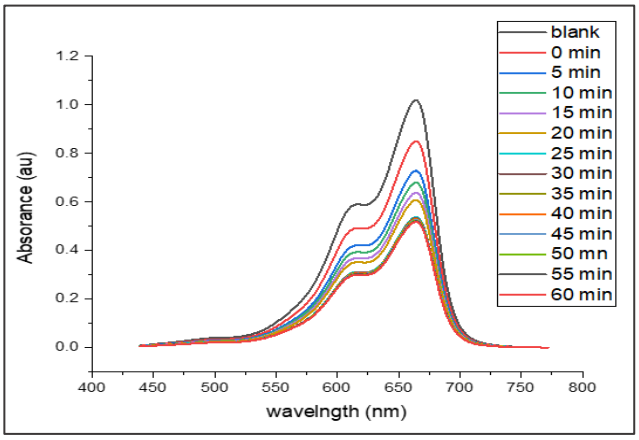

Fig. 9b. Degradation Of Methylene Blue Dye At pH=7 using ZnO/Fe_3O_4 NCs

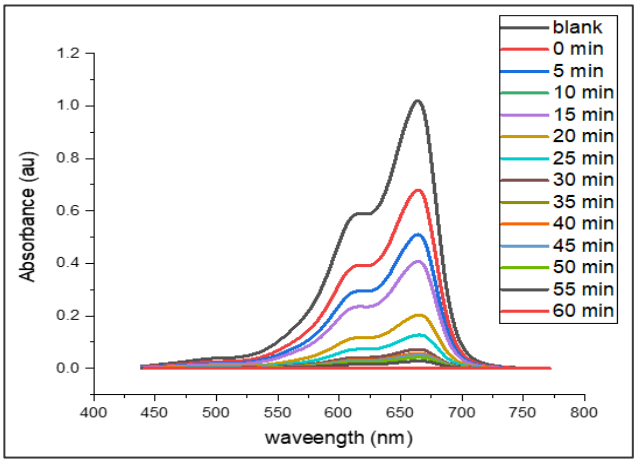

Fig. 9c. Degradation Of Methylene Blue Dye At pH=10 using ZnO/Fe_3O_4 NCs

3.6.2 Time study

Time is the most crucial factor for the degradation of MB dye. Time has a direct relation with the % degradation of MB dye. In this study, NCs showed excellent performance at 60 minutes, which resulted in 99.5 % degradation, as shown in Fig. 10a. degradation increases as time increases. The maximum % degradation was found when the time was reached at 60 minutes, and that was 99.5%, as shown in Histogram Fig.10b. It is cleanly observed that before adding a sample of ZnO/Fe_3O_4 NCsthe color of MB was dark blue, but as we added sample NCs its color from dark blue changed to colorless within 60 minutes as depicted in Fig 10c.

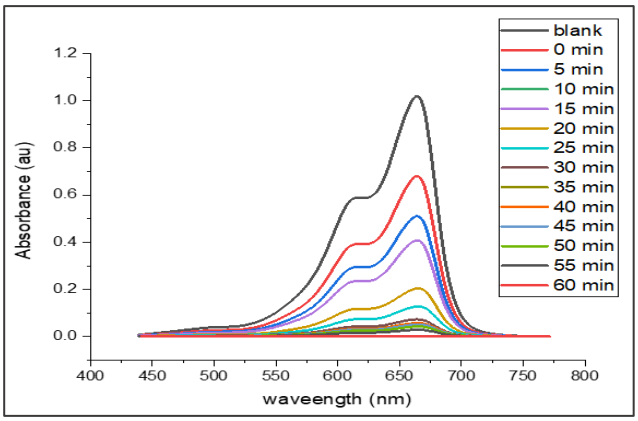

Fig. 10a. % Degradation of MB With Time (0-60min) Using ZnO/Fe_3O_4 NCs At pH = 10

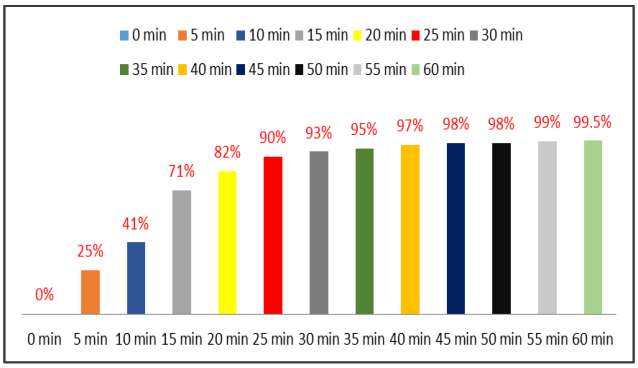

Fig. 10b. Histogram Diagram of % Degradation of MB Using NCs From 0min to 60min

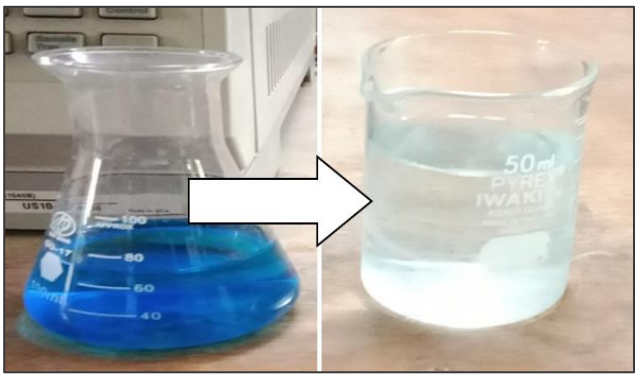

Fig. 10c. Methylene Blue Dye Color Was Changed to Colorless After Addition of ZnO/Fe_3O_4 NCs Within 60min

3.6.3 % Degradation of MB using green synthesized Fe_3O_4 NPs

- The % degradation of MB was calculated using Fe_3O_4 NPs, and the maximum % degradation was found to be around 86% at 60 minutes, as shown in Fig. 11a.

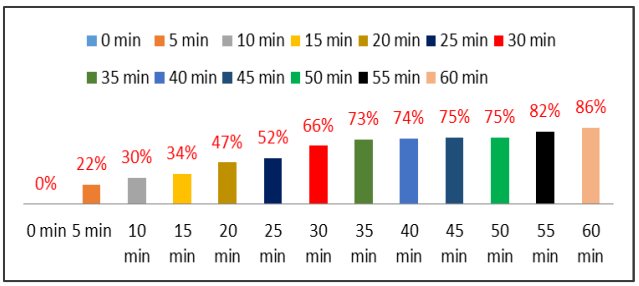

Fig. 11a. Histogram Diagram of% Degradation of MB Using Fe_3O_4 NPs From 0min to 60min

- % degradation of MB using green synthesized ZnO NPs: The % degradation of MB was calculated using ZnO NPs, and the maximum % degradation was around 84% at 60 minutes, as shown in Fig. 11b.

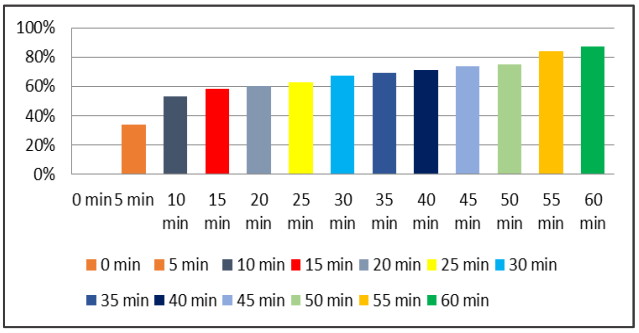

Fig. 11b. Histogram Diagram of% Degradation of MB Using ZnO NPs From 0min to 60min

3.6.4 Comparison of % degradation using ZnO, Fe_3O_4 NPs and ZnO/ Fe_3O_4 NCs

In the relevant study, when separately synthesizing NPs and NCs was applied for % degradation of MB, the maximum % degradation was found in NCs, as shown in Table 1.

Table 1

Comparative study of MB dye conversion % in synthesized NPs and NCs

Nanomaterial catalysts	Time (min)	MB Dye conversion (%)
ZnO	60 min	84
Fe_3O_4	60 min	86
ZnO/ Fe_3O_4	60 min	95.5

3.6.5 Inhibition zone (in mm) of different green synthesized NMs against drug-resistant clinical microbes used in antimicrobial testing

The agar well diffusion method was used to measure the antibacterial activity. Both potato dextrose agar and nutrient agar (for bacteria and Candida, respectively) were put into 25 mL Petri dishes and allowed to harden for 60 minutes. Then, wells in the growth media were carved using a sterile cork borer (6 mm). Then, bacterial or Candida suspensions (tuned to 0.01 OD) of the strains listed above were added to a sterile cotton swab. The cotton swab was used to streak the growth media over the agar plates to inoculate them. Sterile distilled water was used to prepare the samples, and a concentration of 50 mg mL−1 was achieved. Each well was filled with 50 µl of the tested substances or controls. Under LED lighting, the plates were incubated for 48 hours at 37 °C. A negative control was created using distilled water. As indicated in Table 2, the growth inhibition zones' widths were measured in millimeters and percentages.

Table 2

Table representing area of inhibition (mm) and in percentage (%)

Microorganism strains	Test organisms	Zone of inhibition (mm)			
		S. aureus (gram +ve)	S. albus (gram +ve)	E. Coli (gram – ve)	E. Coli (gram – ve)
Concentration in ratios (Zones in mm and %)	ZnO NPs	3:1 (1mm) (25%)	2:2 (-----)	3:1 (-----)	2:2 (-----)
	Fe_3O_4 NPs	3:1 (-----)	2:2 (-----)	3:1 (2mm) (50%)	2:2 (-----)
	ZnO/Fe_3O_4	1:3 (3mm) (75%)	2:2 (-----)	1:3 (1mm) (25%)	2:2 (-----)

In this study, different ratios of samples were taken like in Fig.12 (a), Gram +ve at 1 ratio of ZnO NPs/distilled water 2:2, at 2 ratios of ZnO NPs/distilled water 3:1, at 3 ratios of Fe_3O_4 NPs/distilled water 2:2, at 4 ratios of Fe_3O_4 NPs/distilled water 3:1, at 5 ratios of ZnO/Fe_3O_4 NCs/distilled water 2:2, at 5 ratios of ZnO/Fe_3O_4 NCs/distilled water 3:1, from these all the cultural

media of the Mueller Hinton Agar (M.HA) where all synthesized samples were applied then the maximum zone was observed at marked 5 it means that ratios of ZnO/Fe_3O_4 NCs/distilled water 3:1 have shown best result. In Fig.12 (b), the prepared samples were applied on cultural media of the Mueller Hinton Agar (M.HA) of Gram–ve Escherichia coli (E coli) and Gram +ve Staphylococcus aureus (S. aureus) hereon Gram–ve S. aureus not much effective result was observed, hence, in conclusion, it is noticed that prepared ratios of ZnO/Fe_3O_4 NCs/distilled water 3:1 is more effective for gram +ve S. aureus as compared to Gram –ve E coli [42].

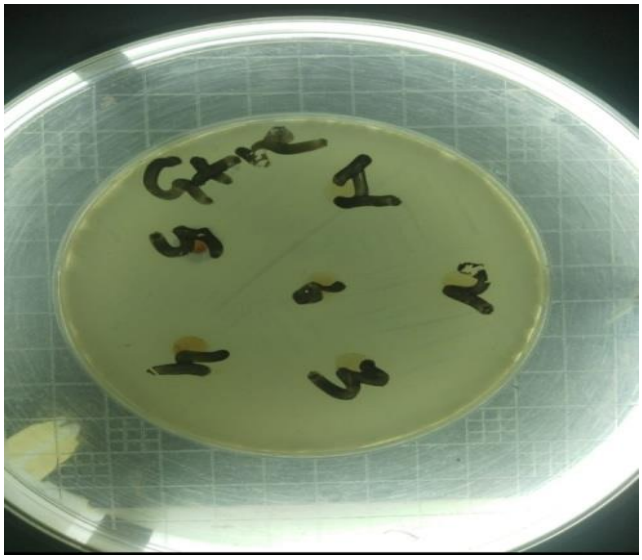

Fig. 12a. Examined Pathogenic Bacteria Of Gram +ve

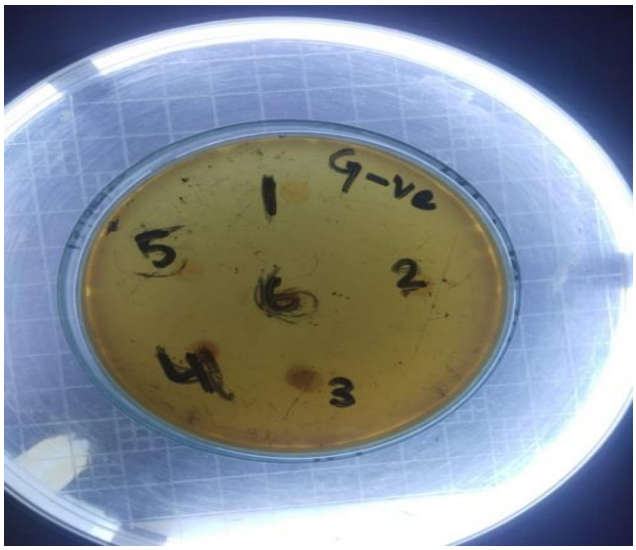

Fig. 12b. Examined Pathogenic Bacteria of Gram –ve From Collected Samples

4. Conclusion

In this study, eco-friendly, greener synthesis of ZnO, Fe_3O_4 NPs, and Fe_3O_4/ZnO NCs was accomplished using the NS seed extract-based aqueous co-precipitation method. Different analytical techniques such as UV-Vis, FTIR, SEM, and XRD were used to characterize the different green synthesized NMs. The fabricated NMs were successfully used to degrade MB and antimicrobial behavior. FTIR peaks further confirmed the formation of ZnO NPs, Fe_3O_4 NPs, and Fe_3O_4/ZnO. SEM analysis showed that most of the particles were agglomerated. XRD showed their average crystalline size was estimated to be 29.52 nm, 22.08 nm, and 12.82 nm for ZnO, Fe_3O_4 NPs, and Fe_3O_4/ZnO NCs, respectively. The prepared NMs showed the best catalytic and antimicrobial activity, but NCs represented outstanding applications for comparing ZnO and Fe_3O_4 NPs. The blue color of the MB dyes was diminished within 60 minutes with % degradation of about 84%, 86%, and 99.5% for ZnO NPs, Fe_3O_4 NPs, and Fe_3O_4/ZnO NCs, and the rate constant was found to be 0.00035, 0.00065, 0.0015 $Lmol^{-1}S^{-1}$. The prepared nanomaterials were applied on cultural media of the Mueller Hinton Agar (M.HA) of Gram-ve Escherichia coli (E coli) and Gram +ve Staphylococcus aureus (S. aureus) here on Gram-ve (S. aureus) not much effective result was observed, hence, in conclusion, it is noticed that prepared ratios of ZnO/Fe_3O_4 NCs/distilled water 3:1 is more effective for G +ve Staphylococcus aureus (S. aureus) as compare to G –ve. E coli. These results demonstrate the effectiveness of Fe_3O_4/ZnO NCs as an excellent catalyst and Gram +ve antimicrobial. This synthesized nanomaterial would be applied effectively for water analysis.

5. Acknowledgments

The authors would like to thank Dr. M. A. Kazi Institute of Chemistry, University of Sindh, Jamshoro, Sindh 76080, Pakistan, for providing a pleasant environment for this study.

6. Conflict Of Interest

The authors declared they have no conflicts of interest.

7. References

[1] S. Bayda, M. Adeel, T. Tuccinardi, M. Cordani, and F. Rizzolio, “The history of nanoscience and nanotechnology: from chemical–physical applications to nanomedicine”, Molecules, vol. 25, no. 1, pp. 112, 2020.

[2] T. Nauroze, S. Ali, L. Kanwal, C. Ara, T. A. Mughal, S. Andleeb, “Ameliorative effect of Nigella sativa conjugated silver nanoparticles against chromium-induced hepatotoxicity and renal toxicity in mice”, Saudi Journal of Biological Science, Vol. 30, no. 3, pp. 103571, 2023.

[3] M. Usman, M. Farooq, A. Wakeel, A. Nawaz, S. A. Cheema, H. Ur Rehman, I. Ashraf, M.

Sanaullah, “Nanotechnology in agriculture: Current status, challenges, and future opportunities”, Science of The Total Environment, Vol. 721, pp. 137778, 2020.

[4] F. Sanchez , K. Sobolev, “Nanotechnology in concrete”, Construction and Building MaterialsVol. 24, no. 11, pp. 2060-2071, 2010.

[5] W. Kooti, Z. Hasanzadeh-Noohi, N. S Ahvazi, M. A. Samani, and D. A. Larky,“Phytochemistry, pharmacology, and therapeutic uses of black seed (Nigella Sativa)”, Chinese Journal of Natural Medicines, Vol. 14, no. 10, pp. 732-745, 2016.

[6] P. Nandhini, K. Surya, V. Kalaiselvi, V. Ramya, and N. Vidhya, “Synthesis and characterization of pure and capped zinc oxide nanoparticles Using Nigella Sativa”, International Journal of Advanced Science and Engineering, Vol. 7, no. 2, pp. 1756-1760, 2020.

[7] M. L. Mathura, J. Gaur, R. Sharma, K. R. Haldiya, “Antidiabetic properties of a spice plant Nigella sativa”, Journal of Endocrinology and Metabolism, Vol. 1, no. 1, pp. 1-8, 2011.

[8] Kyzioł , S. Łukasiewicz, V. Sebastian, P. Kuśtrowski, M. Kozieł, D. Majda, and A. Cierniak, “Towards plant-mediated chemistry – Au nanoparticles obtained using aqueous extract of Rosa damascena and their biological activity in vitro”, Journal of Inorganic Biochemistry, Vol. 214, pp. 111300, 2021.

[9] Koshak , E. Koshak, and M. Heinrich, “Medicinal benefits of Nigella sativa in bronchial asthma: A literature review”, Saudi Pharmaceutical Journal, Vol. 25, no. 8, pp. 1130-1136, 2017.

[10] H. Shafiq, A. Ahmad, T. Masud, and M. Kaleem, “Cardio-protective and anti-cancer therapeutic potential of Nigella sativa”, Iranian Journal of Basic Medical Sciences, Vol. 17, no. 12, pp. 967-979, 2014.

[11] T, El-Naggar, M. E. Carretero C. Arce, and M. P. Gómez-Serranillosa, “Methanol extract of Nigella sativa seed induces changes in the levels of neurotransmitter amino acids in male rat brain regions”, Pharmaceutical Biology, Vol. 55, no. 1, pp. 1415-1422, 2017.

[12] J. E. Hulla1, S. C. Sahu and A. W Hayes, “Nanotechnology: History and future”, Human & Experimental Toxicology, Vol. 34, no. 12, pp. 1318–1321, 2015.

[13] H. Mariamenatu, and E. M. Abdu, “Overconsumption of Omega-6 polyunsaturated fatty acids (PUFAs) versus deficiency of Omega-3 PUFAs in modern-day diets: The disturbing factor for their “balanced antagonistic metabolic functions” in the human body”, Journal of Lipids, Vol. 2021, Article ID 8848161, 15 pages, 2021.

[14] P. Kuppusamy, M. M. Yusoff, G. P. Maniam, and N. Govindan, “Biosynthesis of metallic nanoparticles using plant derivatives and their new avenues in pharmacological applications – An updated report”, Saudi Pharmaceutical Journal, Vol. 24, no. 4, pp. 473-484, 2016.

[15] Y. Bao, J. He, K. Song, J. Guo, X. Zhou, and S. Liu, “Plant-extract-mediated synthesis of metal nanoparticles”, Journal of Chemistry, Vol. 2021, Article ID 6562687, 14 pages, 2021.

[16] E. M. Yimer, K. B. Tuem, A. Karim, N. Ur-Rehman, and F. Anwar, Nigella sativa L. (Black Cumin): A promising natural remedy for wide range of illnesses”, Evidence-based complementary and alternative medicine, Vol. 2019, Article ID 1528635, 16 pages, 2019.

[17] F. Anwar ,F. A. Al-Abbasi, M. S. Nadeem, S. Al-Ghamdi, and A.Kuerban, “Biochemical evaluation of Nigella sativa L. seeds on fluconazole toxicity in Wistar rats”, Journal of Taibah University for Science, Vol. 14, no. 1, pp. 734-741, 2020.

[18] S. Hassan, J. H. Ahmed, and S. S. Al-Haroon, “A study of the effect of Nigella sativa (Black seeds) in isoniazid (INH)-induced hepatotoxicity in rabbits”, Indian Journal of Pharmacology, Vol. 44, no. 6, pp. 678-682, 2012.

[19] Md. A. Hannan, Md. A. Rahman, A. Al M. Sohag, Md. J. Uddin, R. Dash, M. H. Sikder, Md. S. Rahman , B. Timalsina, Y. A. Munni, P. P. Sarker, M. Alam, Md. Mohibbullah , Md. N. Haque, Jahan, Md. T. Hossain, T. Afrin, Md. M. Rahman, Md. T.-Ul-Arif, S. Mitra, D. F. Oktaviani , Md. K. Khan, H. J. Choi 1 , Il S. Moon and B. Kim, Black Cumin (Nigella sativa L.): A comprehensive review on phytochemistry, health benefits, molecular pharmacology, and safety”, Nutrients, 13, 1784, 2021.

[20] N. Shikov, A. N. Tsitsilin, O. N. Pozharitskaya, V. G. Makarov, and M. Heinrich, “Traditional and current food use of wild plants listed in the Russian pharmacopoeia”, Frontiers in Pharmacology, Vol. 8, Article 841, pp. 1-15, 2017.

[21] F. Forouzanfar ,B. S. F. Bazzaz, H. Hosseinzadeh, “Black cumin (Nigella sativa) and its constituent (thymoquinone): a review on antimicrobial effects”, Iranian Journal of Basic Medical Sciences, Vol. 17, no. 12, pp. 929–938, 2014.

[22] M. Mahboubi, “Natural therapeutic approach of Nigella sativa (Black seed) fixed oil in management of Sinusitis”, Integrative Medicine Research, Vol. 7, no. 1, pp. 27-32, 2018.

[23] Singh, P. K. Gautam, A. Verma, V. Singh, P. M. Shivapriya, S. Shivalkar, A. K. Sahoo, S. K. Samanta, “Green synthesis of metallic nanoparticles as effective alternatives to treat antibiotics resistant bacterial infections: A review”, Biotechnology Reports, Vol. 25, Article ID. e00427, 2020.

[24] S. Iravani, “Bacteria in nanoparticle synthesis: Current status and future prospects”, Vol. 2014, Article ID. 359316, 18 pages, 2014.

[25] Pandit, A. Roy, S. Ghotekar, A. Khusro, M. N. Islam, T. B. Emran, S. E. Lam, M. U. Khandaker, D. A. Bradley, “Biological agents for synthesis of nanoparticles and their applications”, Journal of King Saud University – Science, Vol. 34, no. 3, Article ID. 101869, 2022.

[26] M. I. Alkhalaf, R. H. Hussein, and A. Hamza, “Green synthesis of silver nanoparticles by Nigella sativa extract alleviates diabetic neuropathy through anti-inflammatory and antioxidant effects”, Saudi Journal of Biological Sciences, Vol. 27, no. 9, pp. 2410-2419, 2020.

[27] E.M. Awad, and B.R. Binder, “In vitro induction of endothelial cell fibrinolytic alterations by Nigella sativa”, Phytomedicine, Vol. 12, no. 3, pp. 194-202, 2005.

[28] J. M. Alleman, K. Y. Westerhout, M. Hensen, C. Chambers, M. Stoker, S. Long, F. E. van Nooten, “Humanistic and economic burden of painful diabetic peripheral neuropathy in Europe: a review of the literature”, Diabetes Research and Clinical Practice, Vol. 109, no. 2, pp. 215-225, 2015.

[29] M. Yimer, K. B. Tuem, A. Karim, N. Ur-Rehman, and F. Anwar, “Nigella sativa L. (Black Cumin): A Promising Natural Remedy for Wide Range of Illnesses”, Vol. 2019, Artice ID. 1528635. https://doi.org/10.1155/2019/1528635.

[30] B. Lellis, C. Z. F-Polonio, J. A. Pamphile, and J. C. Polonio, “Effects of textile dyes on health and the environment and bioremediation potential of living organisms”, Biotechnology Research and Innovation, Vol. 3, no. 2, pp. 275-290, 2019.

[31] P. Raizada, A. Sudhaik, S. Patial, V. Hasija, A. A. P. Khan, P. Singh, S. Gautam, M. Kaur, and V. H.Nguyen “Engineering nanostructures of CuO-based photo-catalysts for water treatment: Current progress and future challenges”, Arabian Journal of Chemistry, Vol. 13, no. 11, pp. 8424-8457, 2020.

[32] T. Naseem&T. Durrani “The role of some important metal oxide nanoparticles for wastewater and antibacterial applications: A review”, Environmental Chemistry and Ecotoxicology Vol. 3, pp. 59-75, 2021.

[33] V. Batra, I. Kaur, D. Pathania, S.V. Chaudhary “Efficient dye degradation strategies using green synthesized ZnO-based nanoplatforms”, Applied Surface Science Advances Vol. 11, Article ID. 100314, 2021.

[34] Saravanan, P. S. Kumar, R.V. Hemavathy, S. Jeevanantham, M. J. Jawahar, J. P. Neshaanthini, R. Saravanan, “A review on synthesis methods and recent applications of nanomaterial in wastewater treatment: Challenges and future perspectives”, Chemosphere, Vol. 307, no. 1, Article ID. 135713, 2021.

[35] Parita Basnet, T. Inakhunbi Chanu, et al,, “A review on bio-synthesized zinc oxide nanoparticles using plant extracts as reductants and stabilizing agents”, Journal of Photochemistry and Photobiology B: Biology, Vol. 183, June 2018, pp. 201-221, 2018.

[36] Zare, S. Pourseyedi, M. Khatami, E. Darezereshki, “Simple biosynthesis of zinc oxide nanoparticles using nature's source, and it's in vitro bio-activity”, Journal of Molecular Structure, Vol. 1146, pp. 96-103, 2017.

[37] P. B. Chouke, T. Shrirame, A. K. Potbhare, A. Mondal, A. R. Chaudhary, S. Mondal, S. R. Thakare, E. Nepovimova, M. Valis, K. Kuca, “Rohit Sharma i, Ratiram Gomaji Chaudhary Bioinspired metal/metal oxide nanoparticles: A road map to potential applications”, Materials Today Advances, Vol. 16, Artcile ID. 100314, 2022.

[38] Y. Shang, Md. K. Hasan, G. J. Ahammed, M. Li, H. Yin, and J. Zhou, “Applications of Nanotechnology in Plant Growth and Crop Protection: A Review”, Molecules, Vol. 24, no. 14, pages 2558, 2019.

[39] Liu, J. Xu, R. Li, “Chemical and morphological mechanisms of synthesizing rectangular cesium tungsten bronze nanosheets with broadened visible-light absorption and strong photoresponse property”, Materials & Design, Vol. 194, pages- 108955.

[40] Y. B. Chan, V. Selvanathan, L-H. Tey, Md. Akhtaruzzaman, F. H. Anur, S. Djearamane, A. Watanabe, M. Aminuzzaman, “Effect of calcination temperature on structural, morphological and optical properties of copper oxide nanostructures derived from Garcinia mangostana L. Leaf Extract”, Nanomaterials (Basel), Vol. 13, no. 12(20), pages 3589, 2022.

[41] Boutchuen, D. Zimmerman, N. Aich, A. M. Masud, A. Arabshahi, and S. Palchoudhury, “Increased plant growth with hematite nanoparticle fertilizer drop and determining nanoparticle uptake in plants using multimodal approach”, Journal of Nanomaterials, Vol. 2019, Article ID. 6890572, 11 pages, 2019.

[42] R. Al-Tohamy, S. S. Ali, F. Li, K. M. Okash, Y. A.-G. Mahmoud, T. Elsamahy, H. Jiao, Y. Fu, J. Sun, “A critical review on the treatment of dye-containing wastewater: Ecotoxicological and health concerns of textile dyes and possible remediation approaches for environmental safety”, Ecotoxicology and Environmental Safety, Vol. 231, Article ID. 113160, 2022.

